

Observation of $D_s^+ \rightarrow \eta' \mu^+ \nu_\mu$, Precision Test of Lepton Flavor Universality with $D_s^+ \rightarrow \eta^{(\prime)} \ell^+ \nu_\ell$, and First Measurements of $D_s^+ \rightarrow \eta^{(\prime)} \mu^+ \nu_\mu$ Decay Dynamics

- M. Ablikim¹, M. N. Achasov^{13,b}, P. Adlarson⁷³, R. Aliberti³⁴, A. Amoroso^{72A,72C}, M. R. An³⁸, Q. An^{69,56}, Y. Bai⁵⁵, O. Bakina³⁵, I. Balossino^{29A}, Y. Ban^{45,g}, V. Batozskaya^{1,43}, K. Begzsuren³¹, N. Berger³⁴, M. Berlowski⁴³, M. Bertani^{28A}, D. Bettoni^{29A}, F. Bianchi^{72A,72C}, E. Bianco^{72A,72C}, J. Bloms⁶⁶, A. Bortone^{72A,72C}, I. Boyko³⁵, R. A. Briere⁵, A. Brueggemann⁶⁶, H. Cai⁷⁴, X. Cai^{1,56}, A. Calcaterra^{28A}, G. F. Cao^{1,61}, N. Cao^{1,61}, S. A. Cetin^{60A}, J. F. Chang^{1,56}, T. T. Chang⁷⁵, W. L. Chang^{1,61}, G. R. Che⁴², G. Chelkov^{35,a}, C. Chen⁴², Chao Chen⁵³, G. Chen¹, H. S. Chen^{1,61}, M. L. Chen^{1,56,61}, S. J. Chen⁴¹, S. M. Chen⁵⁹, T. Chen^{1,61}, X. R. Chen^{30,61}, X. T. Chen^{1,61}, Y. B. Chen^{1,56}, Y. Q. Chen³³, Z. J. Chen^{25,h}, W. S. Cheng^{72C}, S. K. Choi^{10A}, X. Chu⁴², G. Cibinetto^{29A}, S. C. Coen⁴, F. Cossio^{72C}, J. J. Cui⁴⁸, H. L. Dai^{1,56}, J. P. Dai⁷⁷, A. Dbeysi¹⁹, R. E. de Boer⁴, D. Dedovich³⁵, Z. Y. Deng¹, A. Denig³⁴, I. Denysenko³⁵, M. Destefanis^{72A,72C}, F. De Mori^{72A,72C}, B. Ding^{64,1}, X. X. Ding^{45,g}, Y. Ding³³, Y. Ding³⁹, J. Dong^{1,56}, L. Y. Dong^{1,61}, M. Y. Dong^{1,56,61}, X. Dong⁷⁴, S. X. Du⁷⁹, Z. H. Duan⁴¹, P. Egorov^{35,a}, Y. L. Fan⁷⁴, J. Fang^{1,56}, S. S. Fang^{1,61}, W. X. Fang¹, Y. Fang¹, R. Farinelli^{29A}, L. Fava^{72B,72C}, F. Feldbauer⁴, G. Felici^{28A}, C. Q. Feng^{69,56}, J. H. Feng⁵⁷, K. Fischer⁶⁷, M. Fritsch⁴, C. Fritsch⁶⁶, C. D. Fu¹, Y. W. Fu¹, H. Gao⁶¹, Y. N. Gao^{45,g}, Yang Gao^{69,56}, S. Garbolino^{72C}, I. Garzia^{29A,29B}, P. T. Ge⁷⁴, Z. W. Ge⁴¹, C. Geng⁵⁷, E. M. Gersabeck⁶⁵, A. Gilman⁶⁷, K. Goetzen¹⁴, L. Gong³⁹, W. X. Gong^{1,56}, W. Gradl³⁴, S. Gramigna^{29A,29B}, M. Greco^{72A,72C}, M. H. Gu^{1,56}, Y. T. Gu¹⁶, C. Y. Guan^{1,61}, Z. L. Guan²², A. Q. Guo^{30,61}, L. B. Guo⁴⁰, R. P. Guo⁴⁷, Y. P. Guo^{12,f}, A. Guskov^{35,a}, X. T. H.^{1,61}, W. Y. Han³⁸, X. Q. Hao²⁰, F. A. Harris⁶³, K. K. He⁵³, K. L. He^{1,61}, F. H. Heinsius⁴, C. H. Heinz³⁴, Y. K. Heng^{1,56,61}, C. Herold⁵⁸, T. Holtmann⁴, P. C. Hong^{12,f}, G. Y. Hou^{1,61}, Y. R. Hou⁶¹, Z. L. Hou¹, H. M. Hu^{1,61}, J. F. Hu^{54,i}, T. Hu^{1,56,61}, Y. Hu¹, G. S. Huang^{69,56}, K. X. Huang⁵⁷, L. Q. Huang^{30,61}, X. T. Huang⁴⁸, Y. P. Huang¹, T. Hussain⁷¹, N. Hüskens^{27,34}, W. Imoehl²⁷, M. Irshad^{69,56}, J. Jackson²⁷, S. Jaeger⁴, S. Janchiv³¹, J. H. Jeong^{10A}, Q. Ji¹, Q. P. Ji²⁰, X. B. Ji^{1,61}, X. L. Ji^{1,56}, Y. Y. Ji⁴⁸, Z. K. Jia^{69,56}, P. C. Jiang^{45,g}, S. S. Jiang³⁸, T. J. Jiang¹⁷, X. S. Jiang^{1,56,61}, Y. Jiang⁶¹, J. B. Jiao⁴⁸, Z. Jiao²³, S. Jin⁴¹, Y. Jin⁶⁴, M. Q. Jing^{1,61}, T. Johansson⁷³, X. K.¹, S. Kabana³², N. Kalantar-Nayestanaki⁶², X. L. Kang⁹, X. S. Kang³⁹, R. Kappert⁶², M. Kavatsyuk⁶², B. C. Ke⁷⁹, A. Khokhlov⁶⁶, R. Kiuchi¹, R. Kliemt¹⁴, L. Koch³⁶, O. B. Kolcu^{60A}, B. Kopf⁴, M. Kuessner⁴, A. Kupsc^{43,73}, W. Kühn³⁶, J. J. Lane⁶⁵, J. S. Lange³⁶, P. Larin¹⁹, A. Lavania²⁶, L. Lavezzi^{72A,72C}, T. T. Lei^{69,k}, Z. H. Lei^{69,56}, H. Leithoff³⁴, M. Lellmann³⁴, T. Lenz³⁴, C. Li⁴⁶, C. Li⁴², C. H. Li³⁸, Cheng Li^{69,56}, D. M. Li⁷⁹, F. Li^{1,56}, G. Li¹, H. Li^{69,56}, H. B. Li^{1,61}, H. J. Li²⁰, H. N. Li^{54,i}, Hui Li⁴², J. R. Li⁵⁹, J. S. Li⁵⁷, J. W. Li⁴⁸, Ke Li¹, L. J. Li^{1,61}, L. K. Li¹, Lei Li³, M. H. Li⁴², P. R. Li^{37,j,k}, S. X. Li¹², T. Li⁴⁸, W. D. Li^{1,61}, W. G. Li¹, X. H. Li^{69,56}, X. L. Li⁴⁸, Xiaoyu Li^{1,61}, Y. G. Li^{45,g}, Z. J. Li⁵⁷, Z. X. Li¹⁶, Z. Y. Li⁵⁷, C. Liang⁴¹, H. Liang^{1,61}, H. Liang^{69,56}, H. Liang³³, Y. F. Liang⁵², Y. T. Liang^{30,61}, G. R. Liao¹⁵, L. Z. Liao⁴⁸, J. Libby²⁶, A. Limphirat⁵⁸, D. X. Lin^{30,61}, T. Lin¹, B. J. Liu¹, B. X. Liu⁷⁴, C. Liu³³, C. X. Liu¹, D. Liu^{19,69}, F. H. Liu⁵¹, Fang Liu¹, Feng Liu⁶, G. M. Liu^{54,i}, H. Liu^{37,j,k}, H. B. Liu¹⁶, H. M. Liu^{1,61}, Huanhuan Liu¹, Huihui Liu²¹, J. B. Liu^{69,56}, J. L. Liu⁷⁰, J. Y. Liu^{1,61}, K. Liu¹, K. Y. Liu³⁹, Ke Liu²², L. Liu^{69,56}, L. C. Liu⁴², Lu Liu⁴², M. H. Liu^{12,f}, P. L. Liu¹, Q. Liu⁶¹, S. B. Liu^{69,56}, T. Liu^{12,f}, W. K. Liu⁴², W. M. Liu^{69,56}, X. Liu^{37,j,k}, Y. Liu^{37,j,k}, Y. B. Liu⁴², Z. A. Liu^{1,56,61}, Z. Q. Liu⁴⁸, X. C. Lou^{1,56,61}, F. X. Lu⁵⁷, H. J. Lu²³, J. G. Lu^{1,56}, X. L. Lu¹, Y. Lu⁷, Y. P. Lu^{1,56}, Z. H. Lu^{1,61}, C. L. Luo⁴⁰, M. X. Luo⁷⁸, T. Luo^{12,f}, X. L. Luo^{1,56}, X. R. Lyu⁶¹, Y. F. Lyu⁴², F. C. Ma³⁹, H. L. Ma¹, J. L. Ma^{1,61}, L. L. Ma⁴⁸, M. M. Ma^{1,61}, Q. M. Ma¹, R. Q. Ma^{1,61}, R. T. Ma⁶¹, X. Y. Ma^{1,56}, Y. Ma^{45,g}, F. E. Maas¹⁹, M. Maggiora^{72A,72C}, S. Maldaner⁴, S. Malde⁶⁷, A. Mangoni^{28B}, Y. J. Mao^{45,g}, Z. P. Mao¹, S. Marcello^{72A,72C}, Z. X. Meng⁶⁴, J. G. Messchendorp^{14,62}, G. Mezzadri^{29A}, H. Miao^{1,61}, T. J. Min⁴¹, R. E. Mitchell²⁷, X. H. Mo^{1,56,61}, N. Yu. Muchnoi^{13,b}, Y. Nefedov³⁵, F. Nerling^{19,d}, I. B. Nikolaev^{13,b}, Z. Ning^{1,56}, S. Nisar^{11,l}, Y. Niu⁴⁸, S. L. Olsen⁶¹, Q. Ouyang^{1,56,61}, S. Pacetti^{28B,28C}, X. Pan⁵³, Y. Pan⁵⁵, A. Pathak³³, Y. P. Pei^{69,56}, M. Pelizaeus⁴, H. P. Peng^{69,56}, K. Peters^{14,d}, J. L. Ping⁴⁰, R. G. Ping^{1,61}, S. Plura³⁴, S. Pogodin³⁵, V. Prasad³², F. Z. Qi¹, H. Qi^{69,56}, H. R. Qi⁵⁹, M. Qi⁴¹, T. Y. Qi^{12,f}, S. Qian^{1,56}, W. B. Qian⁶¹, C. F. Qiao⁶¹, J. J. Qin⁷⁰, L. Q. Qin¹⁵, X. P. Qin^{12,f}, X. S. Qin⁴⁸, Z. H. Qin^{1,56}, J. F. Qiu¹, S. Q. Qu⁵⁹, C. F. Redmer³⁴, K. J. Ren³⁸, A. Rivetti^{72C}, V. Rodin⁶², M. Rolo^{72C}, G. Rong^{1,61}, Ch. Rosner¹⁹, S. N. Ruan⁴², N. Salone⁴³, A. Sarantsev^{35,c}, Y. Schelhaas³⁴, K. Schoenning⁷³, M. Scodeggio^{29A,29B}, K. Y. Shan^{12,f}, W. Shan²⁴, X. Y. Shan^{69,56}, J. F. Shangguan⁵³, L. G. Shao^{1,61}, M. Shao^{69,56}, C. P. Shen^{12,f}, H. F. Shen^{1,61}, W. H. Shen⁶¹, X. Y. Shen^{1,61}, B. A. Shi⁶¹, H. C. Shi^{69,56}, J. L. Shi¹², J. Y. Shi¹, Q. Q. Shi⁵³, R. S. Shi^{1,61}, X. Shi^{1,56}, J. J. Song²⁰, T. Z. Song⁵⁷,

W. M. Song^{33,1}, Y. J. Song¹², Y. X. Song^{45,g}, S. Sosio^{72A,72C}, S. Spataro^{72A,72C}, F. Stieler³⁴, Y. J. Su⁶¹, G. B. Sun⁷⁴, G. X. Sun¹, H. Sun⁶¹, H. K. Sun¹, J. F. Sun²⁰, K. Sun⁵⁹, L. Sun⁷⁴, S. S. Sun^{1,61}, T. Sun^{1,61}, W. Y. Sun³³, Y. Sun⁹, Y. J. Sun^{69,56}, Y. Z. Sun¹, Z. T. Sun⁴⁸, Y. X. Tan^{69,56}, C. J. Tang⁵², G. Y. Tang¹, J. Tang⁵⁷, Y. A. Tang⁷⁴, L. Y. Tao⁷⁰, Q. T. Tao^{25,h}, M. Tat⁶⁷, J. X. Teng^{69,56}, V. Thoren⁷³, W. H. Tian⁵⁰, W. H. Tian⁵⁷, Y. Tian^{30,61}, Z. F. Tian⁷⁴, I. Uman^{60B}, B. Wang¹, B. L. Wang⁶¹, Bo Wang^{69,56}, C. W. Wang⁴¹, D. Y. Wang^{45,g}, F. Wang⁷⁰, H. J. Wang^{37,j,k}, H. P. Wang^{1,61}, K. Wang^{1,56}, L. L. Wang¹, M. Wang⁴⁸, Meng Wang^{1,61}, S. Wang^{37,j,k}, S. Wang^{12,f}, T. Wang^{12,f}, T. J. Wang⁴², W. Wang⁵⁷, W. Wang⁷⁰, W. H. Wang⁷⁴, W. P. Wang^{69,56}, X. Wang^{45,g}, X. F. Wang^{37,j,k}, X. J. Wang³⁸, X. L. Wang^{12,f}, Y. Wang⁵⁹, Y. D. Wang⁴⁴, Y. F. Wang^{1,56,61}, Y. H. Wang⁴⁶, Y. N. Wang⁴⁴, Y. Q. Wang¹, Yaqian Wang^{18,1}, Yi Wang⁵⁹, Z. Wang^{1,56}, Z. L. Wang⁷⁰, Z. Y. Wang^{1,61}, Ziwei Wang⁶¹, D. Wei⁶⁸, D. H. Wei¹⁵, F. Weidner⁶⁶, S. P. Wen¹, C. W. Wenzel⁴, U. Wiedner⁴, G. Wilkinson⁶⁷, M. Wolke⁷³, L. Wollenberg⁴, C. Wu³⁸, J. F. Wu^{1,61}, L. H. Wu¹, L. J. Wu^{1,61}, X. Wu^{12,f}, X. H. Wu³³, Y. Wu⁶⁹, Y. J. Wu³⁰, Z. Wu^{1,56}, L. Xia^{69,56}, X. M. Xian³⁸, T. Xiang^{45,g}, D. Xiao^{37,j,k}, G. Y. Xiao⁴¹, H. Xiao^{12,f}, S. Y. Xiao¹, Y. L. Xiao^{12,f}, Z. J. Xiao⁴⁰, C. Xie⁴¹, X. H. Xie^{45,g}, Y. Xie⁴⁸, Y. G. Xie^{1,56}, Y. H. Xie⁶, Z. P. Xie^{69,56}, T. Y. Xing^{1,61}, C. F. Xu^{1,61}, C. J. Xu⁵⁷, G. F. Xu¹, H. Y. Xu⁶⁴, Q. J. Xu¹⁷, W. L. Xu⁶⁴, X. P. Xu⁵³, Y. C. Xu⁷⁶, Z. P. Xu⁴¹, F. Yan^{12,f}, L. Yan^{12,f}, W. B. Yan^{69,56}, W. C. Yan⁷⁹, X. Q. Yan¹, H. J. Yang^{49,e}, H. L. Yang³³, H. X. Yang¹, Tao Yang¹, Y. Yang^{12,f}, Y. F. Yang⁴², Y. X. Yang^{1,61}, Yifan Yang^{1,61}, Z. W. Yang^{37,j,k}, M. Ye^{1,56}, M. H. Ye⁸, J. H. Yin¹, Z. Y. You⁵⁷, B. X. Yu^{1,56,61}, C. X. Yu⁴², G. Yu^{1,61}, T. Yu⁷⁰, X. D. Yu^{45,g}, C. Z. Yuan^{1,61}, L. Yuan², S. C. Yuan¹, X. Q. Yuan¹, Y. Yuan^{1,61}, Z. Y. Yuan⁵⁷, C. X. Yue³⁸, A. A. Zafar⁷¹, F. R. Zeng⁴⁸, X. Zeng^{12,f}, Y. Zeng^{25,h}, Y. J. Zeng^{1,61}, X. Y. Zhai³³, Y. H. Zhan⁵⁷, A. Q. Zhang^{1,61}, B. L. Zhang^{1,61}, B. X. Zhang¹, D. H. Zhang⁴², G. Y. Zhang²⁰, H. Zhang⁶⁹, H. H. Zhang⁵⁷, H. H. Zhang³³, H. Q. Zhang^{1,56,61}, H. Y. Zhang^{1,56}, J. J. Zhang⁵⁰, J. L. Zhang⁷⁵, J. Q. Zhang⁴⁰, J. W. Zhang^{1,56,61}, J. X. Zhang^{37,j,k}, J. Y. Zhang¹, J. Z. Zhang^{1,61}, Jiawei Zhang^{1,61}, L. M. Zhang⁵⁹, L. Q. Zhang⁵⁷, Lei Zhang⁴¹, P. Zhang¹, Q. Y. Zhang^{38,79}, Shuihan Zhang^{1,61}, Shulei Zhang^{25,h}, X. D. Zhang⁴⁴, X. M. Zhang¹, X. Y. Zhang⁵³, X. Y. Zhang⁴⁸, Y. Zhang⁶⁷, Y. T. Zhang⁷⁹, Y. H. Zhang^{1,56}, Yan Zhang^{69,56}, Yao Zhang¹, Z. H. Zhang¹, Z. L. Zhang³³, Z. Y. Zhang⁷⁴, Z. Y. Zhang⁴², G. Zhao¹, J. Zhao³⁸, J. Y. Zhao^{1,61}, J. Z. Zhao^{1,56}, Lei Zhao^{69,56}, Ling Zhao¹, M. G. Zhao⁴², S. J. Zhao⁷⁹, Y. B. Zhao^{1,56}, Y. X. Zhao^{30,61}, Z. G. Zhao^{69,56}, A. Zhemchugov^{35,a}, B. Zheng⁷⁰, J. P. Zheng^{1,56}, W. J. Zheng^{1,61}, Y. H. Zheng⁶¹, B. Zhong⁴⁰, X. Zhong⁵⁷, H. Zhou⁴⁸, L. P. Zhou^{1,61}, X. Zhou⁷⁴, X. K. Zhou⁶, X. R. Zhou^{69,56}, X. Y. Zhou³⁸, Y. Z. Zhou^{12,f}, J. Zhu⁴², K. Zhu¹, K. J. Zhu^{1,56,61}, L. Zhu³³, L. X. Zhu⁶¹, S. H. Zhu⁶⁸, S. Q. Zhu⁴¹, T. J. Zhu^{12,f}, W. J. Zhu^{12,f}, Y. C. Zhu^{69,56}, Z. A. Zhu^{1,61}, J. H. Zou¹, J. Zu^{69,56}

(BESIII Collaboration)

¹ Institute of High Energy Physics, Beijing 100049, People's Republic of China

² Beihang University, Beijing 100191, People's Republic of China

³ Beijing Institute of Petrochemical Technology, Beijing 102617, People's Republic of China

⁴ Bochum Ruhr-University, D-44780 Bochum, Germany

⁵ Carnegie Mellon University, Pittsburgh, Pennsylvania 15213, USA

⁶ Central China Normal University, Wuhan 430079, People's Republic of China

⁷ Central South University, Changsha 410083, People's Republic of China

⁸ China Center of Advanced Science and Technology, Beijing 100190, People's Republic of China

⁹ China University of Geosciences, Wuhan 430074, People's Republic of China

¹⁰ Chung-Ang University, Seoul, 06974, Republic of Korea

¹¹ COMSATS University Islamabad, Lahore Campus, Defence Road, Off Raiwind Road, 54000 Lahore, Pakistan

¹² Fudan University, Shanghai 200433, People's Republic of China

¹³ G.I. Budker Institute of Nuclear Physics SB RAS (BINP), Novosibirsk 630090, Russia

¹⁴ GSI Helmholtzcentre for Heavy Ion Research GmbH, D-64291 Darmstadt, Germany

¹⁵ Guangxi Normal University, Guilin 541004, People's Republic of China

¹⁶ Guangxi University, Nanning 530004, People's Republic of China

¹⁷ Hangzhou Normal University, Hangzhou 310036, People's Republic of China

¹⁸ Hebei University, Baoding 071002, People's Republic of China

¹⁹ Helmholtz Institute Mainz, Staudinger Weg 18, D-55099 Mainz, Germany

²⁰ Henan Normal University, Xinxiang 453007, People's Republic of China

²¹ Henan University of Science and Technology, Luoyang 471003, People's Republic of China

- ²² Henan University of Technology, Zhengzhou 450001, People's Republic of China
²³ Huangshan College, Huangshan 245000, People's Republic of China
²⁴ Hunan Normal University, Changsha 410081, People's Republic of China
²⁵ Hunan University, Changsha 410082, People's Republic of China
²⁶ Indian Institute of Technology Madras, Chennai 600036, India
²⁷ Indiana University, Bloomington, Indiana 47405, USA
- ²⁸ INFN Laboratori Nazionali di Frascati , (A)INFN Laboratori Nazionali di Frascati, I-00044, Frascati, Italy; (B)INFN Sezione di Perugia, I-06100, Perugia, Italy; (C)University of Perugia, I-06100, Perugia, Italy
²⁹ INFN Sezione di Ferrara, (A)INFN Sezione di Ferrara, I-44122, Ferrara, Italy; (B)University of Ferrara, I-44122, Ferrara, Italy
- ³⁰ Institute of Modern Physics, Lanzhou 730000, People's Republic of China
³¹ Institute of Physics and Technology, Peace Avenue 54B, Ulaanbaatar 13330, Mongolia
³² Instituto de Alta Investigación, Universidad de Tarapacá, Casilla 7D, Arica, Chile
³³ Jilin University, Changchun 130012, People's Republic of China
- ³⁴ Johannes Gutenberg University of Mainz, Johann-Joachim-Becher-Weg 45, D-55099 Mainz, Germany
³⁵ Joint Institute for Nuclear Research, 141980 Dubna, Moscow region, Russia
- ³⁶ Justus-Liebig-Universitaet Giessen, II. Physikalisches Institut, Heinrich-Buff-Ring 16, D-35392 Giessen, Germany
³⁷ Lanzhou University, Lanzhou 730000, People's Republic of China
³⁸ Liaoning Normal University, Dalian 116029, People's Republic of China
³⁹ Liaoning University, Shenyang 110036, People's Republic of China
⁴⁰ Nanjing Normal University, Nanjing 210023, People's Republic of China
⁴¹ Nanjing University, Nanjing 210093, People's Republic of China
⁴² Nankai University, Tianjin 300071, People's Republic of China
⁴³ National Centre for Nuclear Research, Warsaw 02-093, Poland
- ⁴⁴ North China Electric Power University, Beijing 102206, People's Republic of China
⁴⁵ Peking University, Beijing 100871, People's Republic of China
⁴⁶ Qufu Normal University, Qufu 273165, People's Republic of China
⁴⁷ Shandong Normal University, Jinan 250014, People's Republic of China
⁴⁸ Shandong University, Jinan 250100, People's Republic of China
- ⁴⁹ Shanghai Jiao Tong University, Shanghai 200240, People's Republic of China
⁵⁰ Shanxi Normal University, Linfen 041004, People's Republic of China
⁵¹ Shanxi University, Taiyuan 030006, People's Republic of China
⁵² Sichuan University, Chengdu 610064, People's Republic of China
⁵³ Soochow University, Suzhou 215006, People's Republic of China
- ⁵⁴ South China Normal University, Guangzhou 510006, People's Republic of China
⁵⁵ Southeast University, Nanjing 211100, People's Republic of China
⁵⁶ State Key Laboratory of Particle Detection and Electronics, Beijing 100049, Hefei 230026, People's Republic of China
- ⁵⁷ Sun Yat-Sen University, Guangzhou 510275, People's Republic of China
- ⁵⁸ Suranaree University of Technology, University Avenue 111, Nakhon Ratchasima 30000, Thailand
⁵⁹ Tsinghua University, Beijing 100084, People's Republic of China
- ⁶⁰ Turkish Accelerator Center Particle Factory Group, (A)Istinye University, 34010, Istanbul, Turkey; (B)Near East University, Nicosia, North Cyprus, 99138, Mersin 10, Turkey
- ⁶¹ University of Chinese Academy of Sciences, Beijing 100049, People's Republic of China
⁶² University of Groningen, NL-9747 AA Groningen, The Netherlands
⁶³ University of Hawaii, Honolulu, Hawaii 96822, USA
⁶⁴ University of Jinan, Jinan 250022, People's Republic of China
- ⁶⁵ University of Manchester, Oxford Road, Manchester, M13 9PL, United Kingdom
⁶⁶ University of Muenster, Wilhelm-Klemm-Strasse 9, 48149 Muenster, Germany
⁶⁷ University of Oxford, Keble Road, Oxford OX13RH, United Kingdom
- ⁶⁸ University of Science and Technology Liaoning, Anshan 114051, People's Republic of China

⁶⁹ University of Science and Technology of China, Hefei 230026, People's Republic of China

⁷⁰ University of South China, Hengyang 421001, People's Republic of China

⁷¹ University of the Punjab, Lahore-54590, Pakistan

⁷² University of Turin and INFN, (A)University of Turin, I-10125, Turin, Italy; (B)University of Eastern Piedmont, I-15121, Alessandria, Italy; (C)INFN, I-10125, Turin, Italy

⁷³ Uppsala University, Box 516, SE-75120 Uppsala, Sweden

⁷⁴ Wuhan University, Wuhan 430072, People's Republic of China

⁷⁵ Xinyang Normal University, Xinyang 464000, People's Republic of China

⁷⁶ Yantai University, Yantai 264005, People's Republic of China

⁷⁷ Yunnan University, Kunming 650500, People's Republic of China

⁷⁸ Zhejiang University, Hangzhou 310027, People's Republic of China

⁷⁹ Zhengzhou University, Zhengzhou 450001, People's Republic of China

^a Also at the Moscow Institute of Physics and Technology, Moscow 141700, Russia

^b Also at the Novosibirsk State University, Novosibirsk, 630090, Russia

^c Also at the NRC "Kurchatov Institute", PNPI, 188300, Gatchina, Russia

^d Also at Goethe University Frankfurt, 60323 Frankfurt am Main, Germany

^e Also at Key Laboratory for Particle Physics, Astrophysics and Cosmology, Ministry of Education; Shanghai Key Laboratory for Particle Physics and Cosmology; Institute of Nuclear and Particle Physics, Shanghai 200240, People's Republic of China

^f Also at Key Laboratory of Nuclear Physics and Ion-beam Application (MOE) and Institute of Modern Physics, Fudan University, Shanghai 200443, People's Republic of China

^g Also at State Key Laboratory of Nuclear Physics and Technology, Peking University, Beijing 100871, People's Republic of China

^h Also at School of Physics and Electronics, Hunan University, Changsha 410082, China

ⁱ Also at Guangdong Provincial Key Laboratory of Nuclear Science, Institute of Quantum Matter, South China Normal University, Guangzhou 510006, China

^j Also at Frontiers Science Center for Rare Isotopes, Lanzhou University, Lanzhou 730000, People's Republic of China

^k Also at Lanzhou Center for Theoretical Physics, Lanzhou University, Lanzhou 730000, People's Republic of China

^l Also at the Department of Mathematical Sciences, IBA, Karachi, Pakistan

By analyzing 7.33 fb^{-1} of e^+e^- annihilation data collected at center-of-mass energies between 4.128 and 4.226 GeV with the BESIII detector, we report the observation of the semileptonic decay $D_s^+ \rightarrow \eta' \mu^+ \nu_\mu$, with a statistical significance larger than 10σ , and the measurements of the $D_s^+ \rightarrow \eta \mu^+ \nu_\mu$ and $D_s^+ \rightarrow \eta' \mu^+ \nu_\mu$ decay dynamics for the first time. The branching fractions of $D_s^+ \rightarrow \eta \mu^+ \nu_\mu$ and $D_s^+ \rightarrow \eta' \mu^+ \nu_\mu$ are determined to be $(2.235 \pm 0.051_{\text{stat}} \pm 0.052_{\text{syst}})\%$ and $(0.801 \pm 0.055_{\text{stat}} \pm 0.028_{\text{syst}})\%$, respectively, with precision improved by factors of 6.0 and 6.6 compared to the previous best measurements. Combined with the results for the decays $D_s^+ \rightarrow \eta e^+ \nu_e$ and $D_s^+ \rightarrow \eta' e^+ \nu_e$, the ratios of the decay widths are examined both inclusively and in several $\ell^+ \nu_\ell$ four-momentum transfer ranges. No evidence for lepton flavor universality violation is found within the current statistics. The products of the hadronic form factors $f_{+,0}^{\eta^{(*)}}(0)$ and the $c \rightarrow s$ Cabibbo-Kobayashi-Maskawa matrix element $|V_{cs}|$ are determined. The results based on the two-parameter series expansion are $f_{+,0}^\eta(0)|V_{cs}| = 0.452 \pm 0.010_{\text{stat}} \pm 0.007_{\text{syst}}$ and $f_{+,0}^{\eta'}(0)|V_{cs}| = 0.504 \pm 0.037_{\text{stat}} \pm 0.012_{\text{syst}}$, which help to constrain present models on $f_{+,0}^{\eta^{(*)}}(0)$. The forward-backward asymmetries are determined to be $\langle A_{\text{FB}}^\eta \rangle = -0.059 \pm 0.031_{\text{stat}} \pm 0.005_{\text{syst}}$ and $\langle A_{\text{FB}}^{\eta'} \rangle = -0.064 \pm 0.079_{\text{stat}} \pm 0.006_{\text{syst}}$ for the first time, which are consistent with the theoretical calculation.

The couplings between the three families of leptons and the gauge bosons are expected to be equal in the standard model (SM). This property is known as lepton flavor universality (LFU). In recent years, however, hints of tensions between experimental measurements and the SM predictions were reported in the semileptonic (SL) B decays [1], the anomalous magnetic moment of the

muon [2, 3], and the Cabibbo angle anomaly [4, 5]. For example, the measured branching fraction (BF) ratios $\mathcal{R}_{D^{(*)}}^{\tau/\ell} = \mathcal{B}_{B \rightarrow \bar{D}^{(*)}\tau^+\nu_\tau}/\mathcal{B}_{B \rightarrow \bar{D}^{(*)}\ell^+\nu_\ell}$ ($\ell = \mu, e$) [6–12] deviate from the SM predictions by 3.3σ [1]. Although these tensions have been explained by various theoretical models [13–24], no definite conclusion is established yet. Precision tests of LFU in different SL decays of heavy

mesons provide deeper insight into these anomalies. Possible LFU in the SL D_s^+ decays is not yet well tested [25], due to poor knowledge of the semimuonic D_s^+ decays. Reference [26] notes that there may indeed be observable LFU violation effects in the SL decays mediated via $c \rightarrow s\ell^+\nu_\ell$. In the SM, the ratio $\mathcal{R}_{\mu/e}^{\eta^{(\prime)}} = \mathcal{B}_{D_s^+ \rightarrow \eta^{(\prime)}\mu^+\nu_\mu}/\mathcal{B}_{D_s^+ \rightarrow \eta^{(\prime)}e^+\nu_e}$ is predicted to be 0.95–0.99 [27–29]. Precision measurements of $D_s^+ \rightarrow \eta^{(\prime)}\mu^+\nu_\mu$ are important to test μ - e LFU with the SL decays $D_s^+ \rightarrow \eta^{(\prime)}\ell^+\nu_\ell$. Especially, the $D_s^+ \rightarrow \eta\ell^+\nu_\ell$ decay is expected to be the most competitive mode in the D_s^+ sector.

Furthermore, measurements of the $D_s^+ \rightarrow \eta^{(\prime)}\ell^+\nu_\ell$ dynamics are important to determine the $c \rightarrow s$ Cabibbo-Kobayashi-Maskawa (CKM) matrix element $|V_{cs}|$ and the vector or scalar hadronic form factors (FFs) $f_{+,0}^{\eta^{(\prime)}}(q^2)$, after incorporating the inputs from the SM global fit [30] or theoretical calculations [28, 29, 31–39]. The obtained results are critical to test the unitarity of the CKM matrix and validate different theoretical calculations on FFs. To date, only the vector FFs of $f_+^{\eta^{(\prime)}}(q^2)$ has been measured by analyzing the $D_s^+ \rightarrow \eta^{(\prime)}e^+\nu_e$ dynamics at BESIII [40, 41]. However, no $f_0^{\eta^{(\prime)}}(q^2)$ is available due to negligible lepton mass in $D_s^+ \rightarrow \eta^{(\prime)}e^+\nu_e$. The $D_s^+ \rightarrow \eta^{(\prime)}\mu^+\nu_\mu$ decays offer unique test-bed to access $f_0^{\eta^{(\prime)}}(q^2)$ besides $|V_{cs}|$ and $f_+^{\eta^{(\prime)}}(q^2)$. Especially, Refs. [29, 33] state that the forward-backward asymmetry parameters ($\langle A_{FB} \rangle$), defined relative to helicity amplitudes, are partially dependent on the expected decay rates and hadronic FFs; and non-zero asymmetries in $D_s^+ \rightarrow \eta^{(\prime)}\mu^+\nu_\mu$ are expected [29, 33]. The obtained $f_0^{\eta^{(\prime)}}(q^2)$ and $\langle A_{FB} \rangle$ are important to validate different theoretical calculations [29, 31–34], thereby improve the precision of lattice quantum chromodynamics (LQCD) calculations on the hadronic FFs of SL D_s^+ decays [32], which are currently suffering large uncertainties compared to their $D^{0(+)}$ counterparts [42–46]. These will reversely help to determine the CKM matrix elements precisely, which are crucial to test the unitarity of the CKM matrix at higher precision [47–50].

Previously, only BESIII reported the BFs of $D_s^+ \rightarrow \eta^{(\prime)}\mu^+\nu_\mu$ [51] with large uncertainties of 20% (51%) using 0.482 fb $^{-1}$ of e^+e^- collision data taken at a center-of-mass energy $E_{CM} = 4.009$ GeV. Using 7.33 fb $^{-1}$ of e^+e^- collision data taken at E_{CM} between 4.128 and 4.226 GeV with the BESIII detector, we report the first observation of $D_s^+ \rightarrow \eta'\mu^+\nu_\mu$, and the BFs of $D_s^+ \rightarrow \eta^{(\prime)}\mu^+\nu_\mu$ are determined with improved precision by about sixfold. Based on these, we test μ - e LFU in $D_s^+ \rightarrow \eta^{(\prime)}\ell^+\nu_\ell$ decays in the full kinematic range and several q^2 intervals. By analyzing the $D_s^+ \rightarrow \eta^{(\prime)}\mu^+\nu_\mu$ dynamics, we determine $f_0^{\eta^{(\prime)}}(q^2)$ and $\langle A_{FB} \rangle$ for the first time. Charge-conjugate modes are implied throughout this Letter.

A description of the design and performance of the

BESIII detector can be found in Ref. [52]. About 83% of the data analyzed in this Letter profits from an upgrade of the end cap time-of-flight system with multi-gap resistive plate chambers with a time resolution of 60 ps [53, 54]. Monte Carlo (MC) simulated events are generated with a GEANT4-based [55] simulation software, which includes the geometric description [56] and a simulation of the response of the detector. An inclusive MC sample with an equivalent luminosity of 40 times that of the data is produced at E_{CM} between 4.128 and 4.226 GeV. It includes open charm processes, initial state radiation (ISR) production of charmonium [$\psi(3770)$, $\psi(3686)$, and J/ψ], $q\bar{q}(q = u, d, s)$ continuum processes, along with Bhabha scattering, $\mu^+\mu^-$, $\tau^+\tau^-$, and $\gamma\gamma$ events. The open charm processes are generated using CONEXC [57]. The effects of ISR and final state radiation are included. Signal MC samples of the SL decays $D_s^+ \rightarrow \eta^{(\prime)}\mu^+\nu_\mu$ are simulated with the two-parameter series expansion model [58], with parameters obtained in this work. The input cross section of $e^+e^- \rightarrow D_s^\pm D_s^{*\mp}$ is taken from Ref. [59]. In the MC generation, known particle decays are generated by EVTGEN [60] with the BFs taken from the Particle Data Group [30], and other modes are generated using LUNDCHARM [61].

In e^+e^- collisions at E_{CM} between 4.128 and 4.226 GeV, the D_s^+ mesons are produced predominantly via $e^+e^- \rightarrow D_s^\pm D_s^{*\mp}$ [62]. Candidates in which one D_s^- is fully reconstructed in one of the fourteen hadronic decay modes, $D_s^- \rightarrow K^+K^-\pi^-$, $K^+K^-\pi^-\pi^0$, $K_S^0K^-$, $K_S^0K^-\pi^0$, $K_S^0K^0\pi^-$, $K_S^0K^+\pi^-\pi^-$, $K_S^0K^-\pi^+\pi^-$, $\pi^+\pi^-\pi^-$, $\eta\gamma\gamma\pi^-$, $\eta\pi^0\pi^+\pi^-\pi^-$, $\eta'_{\eta\gamma\gamma}\pi^+\pi^-\pi^-$, $\eta'_{\gamma\pi^+\pi^-\pi^-}$, $\eta\gamma\gamma\rho^-$, and $\eta\pi^0\pi^+\pi^-\rho^-$, are called the single-tag (ST) D_s^- . Those in which the ST D_s^- , the transition $\gamma(\pi^0)$ of the $D_s^{*\mp}$ decay, and the signal decays of $D_s^+ \rightarrow \eta^{(\prime)}\mu^+\nu_\mu$ are simultaneously reconstructed are called double-tag (DT) events. Based on these, we determine the BF of the signal decay by

$$\mathcal{B}_{\text{sig}} = N_{\text{DT}}/(N_{\text{ST}}^{\text{tot}} \cdot \epsilon_{\gamma(\pi^0)\text{sig}}), \quad (1)$$

where $N_{\text{ST}}^{\text{tot}} = \sum_k N_{\text{ST}}^k$ and N_{DT} are the total ST and DT yields in data summing over tag mode k , and $\epsilon_{\gamma(\pi^0)\text{sig}}$ is the effective signal efficiency of selecting $\gamma(\pi^0)\eta^{(\prime)}\mu^+\nu_\mu$ in the presence of ST D_s^- . The $\epsilon_{\gamma(\pi^0)\text{sig}}$ is the averaged efficiency of $\epsilon_{\gamma\text{sig}}$ and $\epsilon_{\pi^0\text{sig}}$, and estimated by $\sum_k \frac{N_{\text{ST}}^k}{N_{\text{ST}}^{\text{tot}}} \frac{\epsilon_{\text{DT}}^k}{\epsilon_{\text{ST}}^k}$, where ϵ_{ST}^k and ϵ_{DT}^k are the ST and DT efficiencies for the k -th tag mode, respectively.

For each tag mode, the ST yield is extracted from a fit to the corresponding invariant-mass spectrum of the ST candidates. The selection criteria for all ST candidates are the same as Ref. [41], where detailed description can be found. The total ST yield is $N_{\text{ST}}^{\text{tot}} = (817.0 \pm 3.4_{\text{stat}}) \times 10^3$.

In the presence of ST D_s^- , we select candidates

for the transition $\gamma(\pi^0)$ from D_s^{*+} decay and signal $D_s^+ \rightarrow \eta^{(\prime)}\mu^+\nu_\mu$ among the unused particles recoiling against the ST D_s^- . In the signal decay, the η is reconstructed via $\eta \rightarrow \gamma\gamma$ or $\eta \rightarrow \pi^0\pi^+\pi^-$ decay, and the η' is reconstructed via $\eta' \rightarrow \eta\gamma\pi^+\pi^-$ or $\gamma\pi^+\pi^-$ decay. Particle identification (PID) for pions combines the specific ionization information in the multilayer drift chamber and the flight time in the time-of-flight system, and PID for muons further combine the energy deposited in the electromagnetic calorimeter (EMC). Likelihoods under various particle hypotheses (\mathcal{L}_i , $i = e, \pi, \mu$, and K) are calculated. Charged tracks satisfying $\mathcal{L}_\pi > 0.001$, $\mathcal{L}_\pi > \mathcal{L}_K$ are assigned as pion candidates, and satisfying $\mathcal{L}_\mu > 0.001$, $\mathcal{L}_\mu > \mathcal{L}_e$, $\mathcal{L}_\mu > \mathcal{L}_K$, and $E_{\text{EMC}} \in (0.10, 0.28) \text{ GeV}$ are assigned as muon candidates, where E_{EMC} is the energy deposited in the EMC of muon candidates. The selection criteria for the transition $\gamma(\pi^0)$ and $\eta^{(\prime)}$ are the same as those in Ref. [41]. The energy and momentum of the missing neutrino of the signal SL decay are derived as $E_{\nu_\mu} \equiv E_{\text{CM}} - \sum_i E_i$ and $\vec{p}_{\nu_\mu} \equiv -\sum_i \vec{p}_i$, respectively, where E_i and \vec{p}_i are the energy and momentum of the particle i , with i running over the ST D_s^- , transition $\gamma(\pi^0)$, $\eta^{(\prime)}$, and μ^+ .

The yield of signal events is determined by a fit to the distribution of the kinematic variable $\text{MM}^2 \equiv E_{\nu_\mu}^2/c^4 - |\vec{p}_{\nu_\mu}|^2/c^2$. To improve the MM^2 resolution, the candidate tracks, along with the missing neutrino, are subjected to a 3-constraint kinematic fit requiring energy and momentum conservation, constraining the invariant-mass of each D_s^\pm meson to the known D_s^\pm mass [30], and constraining the invariant-mass of the $D_s^- \gamma(\pi^0)$ or $D_s^+ \gamma(\pi^0)$ combination to the known $D_s^{*\pm}$ mass [30]. The combination with the lowest χ^2 is kept. The χ^2 for $D_s^+ \rightarrow \eta'\gamma\pi^+\pi^-\mu^+\nu_\mu$ is required to be less than 30 to further suppress the non- $D_s^\pm D_s^{*\mp}$ backgrounds.

To suppress the backgrounds, the energy of any unused shower ($E_{\gamma \text{ extra}}^{\max}$) in an event is required to be less than 0.2 GeV. The DT candidates are vetoed if they contain any additional charged tracks ($N_{\text{extra}}^{\text{char}}$) or π^0 reconstructed by two unused photons ($N_{\text{extra}}^{\pi^0}$). To further reject the peaking backgrounds from $D_s^+ \rightarrow \eta^{(\prime)}\pi^+$ and $D_s^+ \rightarrow \eta^{(\prime)}\pi^+\pi^0$, the invariant-masses of $\eta^{(\prime)}\mu^+$, $M_{\eta^{(\prime)}\mu^+}$, are required to be less than $1.8 \text{ GeV}/c^2$ for both $D_s^+ \rightarrow \eta\mu^+\nu_\mu$ and $D_s^+ \rightarrow \eta'\mu^+\nu_\mu$, and the invariant-masses of $\eta^{(\prime)}\nu_\mu$, $M_{\eta^{(\prime)}\nu_\mu}$, are required to be greater than $0.97 \text{ GeV}/c^2$ and $1.27 \text{ GeV}/c^2$ for $D_s^+ \rightarrow \eta\mu^+\nu_\mu$ and $D_s^+ \rightarrow \eta'\mu^+\nu_\mu$, respectively.

After imposing all above selection criteria, the resulting MM^2 distributions of the accepted candidates for different signal decay modes are exhibited in Fig. 1. For $D_s^+ \rightarrow \eta^{(\prime)}\mu^+\nu_\mu$, the signal yield is extracted from a simultaneous unbinned maximum-likelihood fit to the MM^2 spectra for the two η or η' reconstruction modes, with BFs constrained to be the same in the fit. The signal, peaking backgrounds of $D_s^+ \rightarrow \eta^{(\prime)}\pi^+(\pi^0)$, and

other background shapes are modeled by the individual simulated shapes taken from the inclusive MC sample. The signal and peaking background shapes are convolved with a Gaussian resolution function to account for the differences between data and simulation. The yields of the peaking backgrounds are fixed to the expectation from simulation, and the other yields are left free. The obtained signal efficiencies, signal yields, and resultant BFs are shown in Table 1. The signal efficiencies have been corrected for small data-MC differences (overall factor $f^{\text{cor}} = 0.992 \sim 1.018$) in the η, π^0 reconstruction, μ^+ PID, requirements of $E_{\gamma, \text{extra}}^{\max}, N_{\text{extra}}^{\text{char}}, N_{\text{extra}}^{\pi^0}$, $M_{\eta^{(\prime)}\mu^+}$, $M_{\eta^{(\prime)}\nu_\mu}$, and χ^2 .

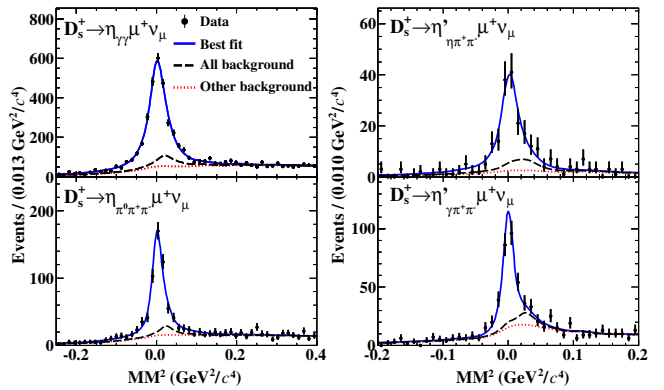


Fig. 1. Simultaneous fits to the MM^2 distributions of the accepted candidates for $D_s^+ \rightarrow \eta^{(\prime)}\mu^+\nu_\mu$. Points with error bars are data, solid curves are the best fits, differences between dashed and dotted curves are the $D_s^+ \rightarrow \eta^{(\prime)}\pi^+(\pi^0)$ peaking backgrounds, and dotted curves are the other backgrounds.

Table 1. Signal efficiencies ($\epsilon_{\gamma(\pi^0)\text{sig}}$), signal yields (N_{DT}), and obtained BFs (\mathcal{B}_{sig}). Efficiencies are averaged by $\epsilon_{\gamma\text{sig}}$ and $\epsilon_{\pi^0\text{sig}}$, and include the BFs of the $\eta^{(\prime)}$ and $D_s^{*\mp}$ sub-decays. Numbers in the first and second parentheses are the most significant digits of the statistical and systematic uncertainties, respectively.

Decay	$\eta\mu^+\nu_\mu$	$\eta'\mu^+\nu_\mu$
$\eta^{(\prime)}$ decay	$\gamma\gamma$ $\pi^0\pi^+\pi^-$	$\eta\pi^+\pi^-$ $\gamma\pi^+\pi^-$
$\epsilon_{\gamma(\pi^0)\text{sig}} (\%)$	14.06(02) 2.89(01)	2.27(01) 3.64(01)
N_{DT}	2567 528	149 238
$\mathcal{B}_{\text{sig}} (\%)$	2.235(51)(52)	0.801(55)(28)

The systematic uncertainties in the BF measurements are listed in Table 1 of Ref. [63] and are discussed below.

The uncertainty in the ST D_s^- yields is studied by examining the change of the ST D_s^- yields by varying the matched angle for signal shape and the order of Chebychev polynomial for background shape. The uncertainties in the tracking or PID efficiencies of π^\pm

from the secondary $\eta^{(\prime)}$ decay and μ^+ from primary D_s^+ decays are studied with the control samples of $e^+e^- \rightarrow K^+K^-\pi^+\pi^-$ and $e^+e^- \rightarrow \gamma\mu^+\mu^-$, respectively. The uncertainty of the π^0 or η reconstruction is assigned by studying the control sample of $e^+e^- \rightarrow K^+K^-\pi^+\pi^-\pi^0$. The uncertainty in the reconstruction of transition $\gamma(\pi^0)$ from D_s^{*+} is studied with the control sample of $J/\psi \rightarrow \pi^0\pi^+\pi^-$ [64]. The uncertainty from the selection of the transition $\gamma(\pi^0)$ from D_s^{*+} with the smallest $|\Delta E|$ method is estimated by using the control samples of $D_s^+ \rightarrow K^+K^-\pi^+$ and $D_s^+ \rightarrow \eta\pi^+\pi^0$.

The uncertainties due to the signal model are estimated by comparing the DT efficiencies by varying the input hadronic FFs measured by $\pm 1\sigma$. The uncertainties due to the $M_{\eta^{(\prime)}\mu^+}$ and $M_{\eta^{(\prime)}\nu_\mu}$ requirements are estimated by using the DT events of $D_s^+ \rightarrow \eta^{(\prime)}e^+\nu_e$. The uncertainties from the $\eta^{(\prime)}$ reconstruction are estimated by analyzing the control sample of $J/\psi \rightarrow \phi\eta^{(\prime)}$. The systematic uncertainties in the MM² fit are studied by repeating the fits with different signal and background shapes. The uncertainty in the peaking background yield is propagated by varying its size by $\pm 1\sigma$ of the corresponding BF [30].

The uncertainties due to different multiplicities of tag environments [65] are assigned by studying of data-MC

efficiency differences. The uncertainty due to the finite MC statistics, which is dominated by that of the DT efficiency, is considered as a systematic uncertainty.

The uncertainties of the E_γ^{\max} , $N_{\text{extra}}^{\pi^0}$, and N_{extra}^{η} requirements are analyzed with the DT events of $D_s^+ \rightarrow \eta^{(\prime)}\pi^+(\pi^0)$ and $D_s^+ \rightarrow \eta^{(\prime)}e^+\nu_e$. The uncertainties of the χ^2 requirements for $D_s^+ \rightarrow \eta'_{\gamma\pi^+\pi^-}\mu^+\nu_\mu$ are studied with the DT events of $D_s^+ \rightarrow \eta'_{\gamma\pi^+\pi^-}\pi^+$ and $D_s^+ \rightarrow \eta'_{\gamma\pi^+\pi^-}e^+\nu_e$. The uncertainties due to the quoted BFs of $\eta^{(\prime)}$ and D_s^{*+} decays are taken from Ref. [30].

The correlated and uncorrelated systematic uncertainties between the two $\eta^{(\prime)}$ decay modes are summarized in top and bottom section of Table 1 in Ref [63]. The combined systematic uncertainties are 2.3% for $D_s^+ \rightarrow \eta\mu^+\nu_\mu$ and 3.5% for $D_s^+ \rightarrow \eta'\mu^+\nu_\mu$, taking into account correlated and uncorrelated systematic uncertainties with the method described in Ref. [66].

The decay dynamics of $D_s^+ \rightarrow \eta^{(\prime)}\mu^+\nu_\mu$ are investigated by dividing individual candidate events into $m = 8(3)$ intervals of q^2 and performing a least- χ^2_{FF} fit to the measured ($\Delta\Gamma_{\text{msr}}^i$) and theoretically expected ($\Delta\Gamma_{\text{th}}^i$) partial decay rates in the i -th q^2 interval. The $\Delta\Gamma_{\text{th}}^i \equiv \int_i \frac{d\Gamma}{dq^2} dq^2$ relate to the hadronic FF via [33]

$$\frac{d\Gamma}{dq^2} = \frac{G_F^2 |V_{cs}|^2}{24\pi^3} \frac{(q^2 - m_\mu^2)^2 |p_{\eta^{(\prime)}}|}{q^4 m_{D_s^+}^2} \left[\left(1 + \frac{m_\mu^2}{2q^2}\right) m_{D_s^+}^2 |p_{\eta^{(\prime)}}|^2 |f_+^{\eta^{(\prime)}}(q^2)|^2 + \frac{3m_\mu^2}{8q^2} (m_{D_s^+}^2 - m_{\eta^{(\prime)}}^2)^2 |f_0^{\eta^{(\prime)}}(q^2)|^2 \right], \quad (2)$$

where G_F is the Fermi coupling constant [30], $|p_{\eta^{(\prime)}}|$ is the momentum of $\eta^{(\prime)}$ in the D_s^+ rest frame, $m_{\mu(\eta^{(\prime)})}$ is the $\mu^+(\eta^{(\prime)})$ mass. The hadronic FFs $f_+^{\eta^{(\prime)}}(q^2)$ are parameterized with a two-parameter series expansion [67]. We fix the pole mass at the known D_s^{*+} mass [30]. The similar formulas are applied for $f_0^{\eta^{(\prime)}}(q^2)$ but with one-parameter series expansion due to much less contribution, and with the pole mass replaced with $m_{D_{s0}^*(2317)^+}$ [30].

The $\Delta\Gamma_{\text{msr}}^i$ are determined by $\Delta\Gamma_{\text{msr}}^i = \frac{N_{\text{prd}}^i}{\tau_{D_s^+} \cdot N_{\text{ST}}^{\text{tot}}}$, where $\tau_{D_s^+}$ is the D_s^+ meson lifetime [30, 68] and $N_{\text{prd}}^i = \sum_j (\epsilon^{-1})_{ij} N_{\text{DT}}^j$ is the corresponding produced signal yield. The observed signal yield (N_{DT}^j) is obtained from a similar fit of the corresponding MM² distribution. The signal efficiency matrix (ϵ_{ij}) is determined via $\epsilon_{ij} = \sum_k \left[(1/N_{\text{ST}}^{\text{tot}}) \cdot (N_{\text{DT}}^{ij}/N_{\text{gen}}^j)_k \cdot (N_{\text{ST}}^k/\epsilon_{\text{ST}}^k) \cdot f^{\text{cor}} \right]$, where N_{gen}^j is the total signal yield produced in the j -th q^2 interval, N_{rec}^{ij} is the number of events generated in the j -th q^2 interval but reconstructed in the i -th q^2 interval, and k sums over all tag modes. Details of q^2 divisions,

the weighted signal efficiency matrices, N_{DT}^i , N_{prd}^i , and $\Delta\Gamma_{\text{msr}}^i$ of different q^2 intervals for $D_s^+ \rightarrow \eta\mu^+\nu_\mu$ and $D_s^+ \rightarrow \eta'\mu^+\nu_\mu$ are shown in Tables 2-5 of Ref. [63], respectively.

The statistical and systematic covariance matrices are constructed as Ref. [41], which are shown in Tables 6-7 of Ref. [63]. The systematic covariance matrices include with those uncertainties from the BF measurements, along with the D_s^+ lifetime [30, 68].

For each signal decay, we perform a simultaneous fit on the differential decay rates measured by the two $\eta^{(\prime)}$ sub-decays, where the two modes are constrained to have same parameters for the hadronic FF. Figures 2(a,b) show the fits to the differential decay rates. The obtained parameters of hadronic FFs are summarized in Table 2. Figure 3 shows the projections to the extracted $f_+^{\eta^{(\prime)}}(q^2)$, as well as the comparison of $f_{+,0}^{\eta^{(\prime)}}(q^2)$ and various theoretical calculations. Taking $|V_{cs}|$ from the SM global fit [30] as input, we determine $f_{+,0}^{\eta}(0) = 0.465 \pm 0.010_{\text{stat}} \pm 0.007_{\text{syst}}$ and $f_{+,0}^{\eta'}(0) = 0.518 \pm 0.038_{\text{stat}} \pm 0.012_{\text{syst}}$. Conversely, by taking the $f_+^{\eta^{(\prime)}}(0)$ predicted by theory [31] as inputs, we

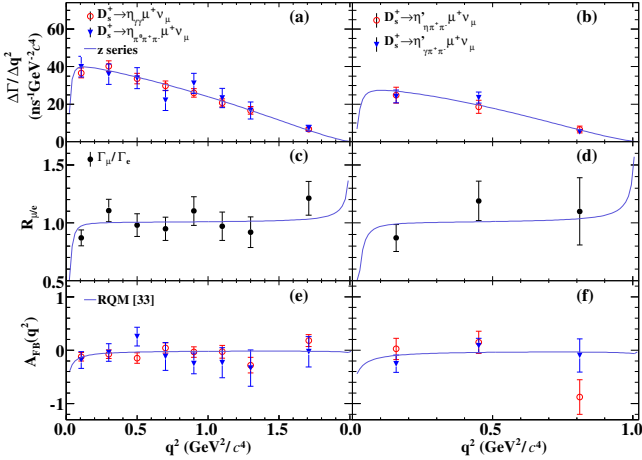


Fig. 2. (a,b) Fits to $\Delta\Gamma_{\text{msr}}^i$. (c,d) The measured $\mathcal{R}_{\mu/e}$ combining the two signal channels in each q^2 interval. (e,f) Comparisons of the measured A_{FB} and theoretical predication [33]. Red circles, blue triangles, and black points with error bars are data; the error bars combine both statistical and systematic uncertainties.

Table 2. Fitted parameters of hadronic FFs. Quantities in the first (second) parentheses are the least two significant digits of statistical (systematic) uncertainties. NDF is the number of degrees of freedom.

Decay	$f_{+,0}^{\eta^{(\prime)}}(0) V_{cs} $	r_1	$\chi_{\text{FF}}^2/\text{NDF}$
$D_s^+ \rightarrow \eta\mu^+\nu_\mu$	$0.452(10)(07)$	$-2.9(06)(02)$	$5.1/14$
$D_s^+ \rightarrow \eta'\mu^+\nu_\mu$	$0.504(37)(12)$	$-10.8(53)(14)$	$2.3/4$

obtain $|V_{cs}|_\eta = 0.913 \pm 0.020_{\text{stat}} \pm 0.014_{\text{syst}} {}^{+0.055}_{-0.053\text{theo}}$ and $|V_{cs}|_{\eta'} = 0.904 \pm 0.067_{\text{stat}} \pm 0.021_{\text{syst}} {}^{+0.076}_{-0.073\text{theo}}$, where the third uncertainties originate from the input FFs. The obtained $f_{+,0}^{\eta^{(\prime)}}(0)$ are consistent with the relativistic quark model, QCD light-cone, and QCD sum rule calculations [28, 31, 33, 35–37]. They disfavor the lattice QCD, covariant light-cone, and covariant confined quark model calculations [29, 32, 34, 38, 39] by more than 4σ .

Combining the BFs measured in this work with our measurements $\mathcal{B}_{D_s^+ \rightarrow \eta e^+\nu_e} = (2.255 \pm 0.039_{\text{stat}} \pm 0.051_{\text{syst}})\%$ and $\mathcal{B}_{D_s^+ \rightarrow \eta' e^+\nu_e} = (0.810 \pm 0.038_{\text{stat}} \pm 0.024_{\text{syst}})\%$ [41], we obtain $\mathcal{R}_{\mu/e}^\eta = 0.991 \pm 0.029_{\text{stat}} \pm 0.016_{\text{syst}}$ and $\mathcal{R}_{\mu/e}^{\eta'} = 0.988 \pm 0.082_{\text{stat}} \pm 0.031_{\text{syst}}$, which are consistent with the SM predictions [27–29]. In addition, we examine the $\mathcal{R}_{\mu/e}^\eta$ and $\mathcal{R}_{\mu/e}^{\eta'}$ in different q^2 intervals after considering the correlated uncertainties, with results shown in Figs. 2(c,d); these are also consistent with the SM predictions.

The forward-backward asymmetry parameter A_{FB} is defined as $A_{\text{FB}}(q^2) = \frac{\int_1^1 d\cos\theta_\ell d\Gamma/d\cos\theta_\ell - \int_{-1}^0 d\cos\theta_\ell d\Gamma/d\cos\theta_\ell}{\int_1^1 d\cos\theta_\ell d\Gamma/d\cos\theta_\ell + \int_{-1}^0 d\cos\theta_\ell d\Gamma/d\cos\theta_\ell}$, where θ_ℓ is

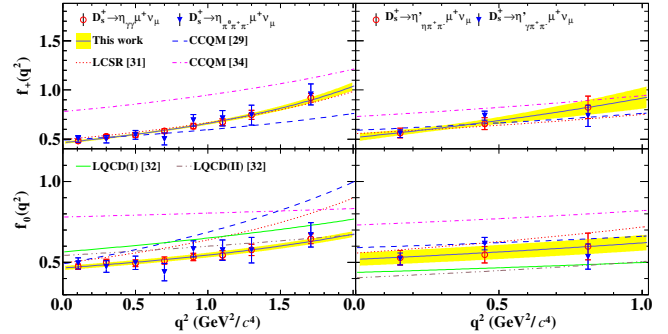


Fig. 3. Projections of the fits on $f_{+,0}^{\eta^{(\prime)}}(q^2)$. Red circles and blue triangles with error bars are data, the yellow bands are the $\pm 1\sigma$ limits of fitted parameters, and the curves in different colors are from various theoretical calculations described in the legend.

the angle between the momentum of the μ^+ in the rest frame of the W -boson and the direction to the W -boson momentum in the rest frame of D_s^+ . The measured A_{FB} in various q^2 intervals are shown in Figs. 2(e,f). The averaged $\langle A_{\text{FB}} \rangle$ are determined to be $-0.059 \pm 0.031_{\text{stat}} \pm 0.005_{\text{syst}}$ for $D_s^+ \rightarrow \eta\mu^+\nu_\mu$ and $-0.064 \pm 0.079_{\text{stat}} \pm 0.006_{\text{syst}}$ for $D_s^+ \rightarrow \eta'\mu^+\nu_\mu$, which are consistent with theoretical predictions [29, 33].

In summary, we present for the first time the observation of $D_s^+ \rightarrow \eta'\mu^+\nu_\mu$ with statistical significance greater than 10σ and the studies of $D_s^+ \rightarrow \eta^{(\prime)}\mu^+\nu_\mu$ dynamics. The BFs of $D_s^+ \rightarrow \eta\mu^+\nu_\mu$ and $D_s^+ \rightarrow \eta'\mu^+\nu_\mu$ are measured with precision improved by about sixfold over the previous best measurements [30]. Combining with the BESIII measurements of $D_s^+ \rightarrow \eta^{(\prime)}e^+\nu_e$ [41], we calculate the $\mathcal{R}_{\mu/e}^{\eta^{(\prime)}}$ ratios in separate q^2 intervals and in the full range. No significant evidence of LFU violation is found with current statistics.

By analyzing the dynamics of these decays, we determine the hadronic FFs of $f_{+,0}^{\eta^{(\prime)}}(0)$, $|V_{cs}|$, the shapes of $f_{+,0}^{\eta^{(\prime)}}(q^2)$, and forward-backward asymmetry parameters of $\langle A_{\text{FB}} \rangle$. The obtained $f_{+,0}^{\eta^{(\prime)}}(q^2)$ lineshapes offer crucial data to calibrate the q^2 dependent FFs from different theories for the first time. Unlike the comparable FFs in the SL decays mediated via $c \rightarrow d e^+\nu_e$ [69], the $D_s^+ \rightarrow \eta$ FF measured in this work deviate from $f_{+,0}^{D \rightarrow K}(0) = 0.7327 \pm 0.0049$ obtained via $D^0 \rightarrow K^- \mu^+\nu_\mu$ [70] by more than 5σ . This rules out the expectation for comparable FFs for $D^{0(+)} \rightarrow \bar{K}\mu^+\nu_\mu$ and $D_s^+ \rightarrow \eta\mu^+\nu_\mu$ [47], but supports that the spectator quarks play important role in FFs due to effects of confinement in the considered weak transitions and the SU(4) asymmetry breaking [71].

The authors thank Prof. Haibing Fu, Prof. Shan Cheng, Prof. Xianwei Kang, and Prof. Khlopov for helpful discussions. The BESIII Collaboration thanks the staff of BEPCII and the IHEP computing center

for their strong support. This work is supported in part by National Key R&D Program of China under Contracts No. 2020YFA0406400, No. 2023YFA1606000, No. 2023YFA1606704, and No. 2020YFA0406300; National Natural Science Foundation of China (NSFC) under Contracts No. 12305089, No. 12375092, No. 11635010, No. 11735014, No. 11835012, No. 11935015, No. 11935016, No. 11935018, No. 11961141012, No. 12022510, No. 12025502, No. 12035009, No. 12035013, No. 12061131003, No. 12192260, No. 12192261, No. 12192262, No. 12192263, No. 12192264, No. 12192265; the Chinese Academy of Sciences (CAS) Large-Scale Scientific Facility Program; the CAS Center for Excellence in Particle Physics (CCEPP); Joint Large-Scale Scientific Facility Funds of the NSFC and CAS under Contract No. U1932102, U1832207; CAS Key Research Program of Frontier Sciences under Contracts Nos. QYZDJ-SSW-SLH003, QYZDJ-SSW-SLH040; 100 Talents Program of CAS; Jiangsu Funding Program for Excellent Postdoctoral Talent under Contracts No. 2023ZB833; Project funded by China Postdoctoral Science Foundation under Contracts No. 2023M732547; The Institute of Nuclear and Particle Physics (INPAC) and Shanghai Key Laboratory for Particle Physics and Cosmology; ERC under Contract No. 758462; European Union's Horizon 2020 research and innovation programme under Marie Skłodowska-Curie grant agreement under Contract No. 894790; German Research Foundation DFG under Contracts Nos. 443159800, 455635585, Collaborative Research Center CRC 1044, FOR5327, GRK 2149; Istituto Nazionale di Fisica Nucleare, Italy; Ministry of Development of Turkey under Contract No. DPT2006K-120470; National Research Foundation of Korea under Contract No. NRF-2022R1A2C1092335; National Science and Technology fund; National Science Research and Innovation Fund (NSRF) via the Program Management Unit for Human Resources & Institutional Development, Research and Innovation under Contract No. B16F640076; Polish National Science Centre under Contract No. 2019/35/O/ST2/02907; Suranaree University of Technology (SUT), Thailand Science Research and Innovation (TSRI), and National Science Research and Innovation Fund (NSRF) under Contract No. 160355; The Royal Society, UK under Contract No. DH160214; The Swedish Research Council; U. S. Department of Energy under Contract No. DE-FG02-05ER41374.

-
- [1] Y. S. Amhis *et al.* (HFLAV Collaboration), *Phys. Rev. D* **107**, 052008 (2023).
- [2] B. Abi *et al.* (Muon g-2 Collaboration), *Phys. Rev. Lett.* **126**, 141801 (2021).
- [3] G. W. Bennett *et al.* (Muon g-2 Collaboration), *Phys. Rev. D* **73**, 072003 (2006).
- [4] A. M. Coutinho, A. Crivellin and C. A. Manzari, *Phys. Rev. Lett.* **125**, 071802 (2020).
- [5] A. Crivellin and M. Hoferichter, *Phys. Rev. Lett.* **125**, 111801 (2020).
- [6] J. P. Lees *et al.* (BaBar Collaboration), *Phys. Rev. Lett.* **109**, 101802 (2012).
- [7] J. P. Lees *et al.* (BaBar Collaboration), *Phys. Rev. D* **88**, 072012 (2013).
- [8] R. Aaij *et al.* (LHCb Collaboration), *Phys. Rev. Lett.* **115**, 111803 (2015).
- [9] M. Huschle *et al.* (Belle Collaboration), *Phys. Rev. D* **92**, 072014 (2015).
- [10] Y. Sato *et al.* (Belle Collaboration), *Phys. Rev. D* **94**, 072007 (2016).
- [11] G. Caria *et al.* (Belle Collaboration), *Phys. Rev. Lett.* **124**, 161803 (2020).
- [12] R. Aaij *et al.* (LHCb Collaboration), *Phys. Rev. Lett.* **131**, 111802 (2023).
- [13] P. S. Bhupal Dev, R. Mohanta, S. Patra and S. Sahoo, *Phys. Rev. D* **102**, 095012 (2020).
- [14] T. Nomura and H. Okada, *Phys. Rev. D* **104**, 035042 (2021).
- [15] M. Bordone, G. Isidori and A. Pattori, *Eur. Phys. J. C* **76**, 440 (2016).
- [16] W. Altmannshofer, P. Stangl and D. M. Straub, *Phys. Rev. D* **96**, 055008 (2017).
- [17] A. Crivellin, D. Müller and T. Ota, *JHEP* **09**, 040 (2017).
- [18] D. Bećirević, S. Fajfer, N. Košnik and O. Sumensari, *Phys. Rev. D* **94**, 115021 (2016).
- [19] S. Fajfer, J. F. Kamenik and I. Nisandžić, *Phys. Rev. D* **85**, 094025 (2012).
- [20] S. Fajfer, J. F. Kamenik, I. Nisandžić and J. Zupan, *Phys. Rev. Lett.* **109**, 161801 (2012).
- [21] A. Celis *et al.*, *JHEP* **1301**, 054 (2013).
- [22] A. Crivellin, G. D'Ambrosio and J. Heeck, *Phys. Rev. Lett.* **114**, 151801 (2015).
- [23] A. Crivellin, J. Heeck and P. Stoffer, *Phys. Rev. Lett.* **116**, 081801 (2016).
- [24] M. Bauer and M. Neubert, *Phys. Rev. Lett.* **116**, 141802 (2016).
- [25] B. C. Ke, J. Koponen, H. B. Li and Y. H. Zheng, *Ann. Rev. Nucl. Part. Sci.* **73**, 285 (2023).
- [26] S. Fajfer, I. Nisandžić and U. Roječ, *Phys. Rev. D* **91**, 094009 (2015).
- [27] H. Y. Cheng and X. W. Kang, *Eur. Phys. J. C* **77**, 587 (2017), [erratum: *Eur. Phys. J. C* **77**, 863 (2017).]
- [28] D. D. Hu, H. B. Fu, T. Zhong, L. Zeng, W. Cheng and X. G. Wu, *Eur. Phys. J. C* **82**, 12 (2022).
- [29] M. A. Ivanov, J. G. Körner, J. N. Pandya, P. Santorelli, N. R. Soni and C. T. Tran, *Front. Phys. (Beijing)* **14**, 64401 (2019).
- [30] R. L. Workman *et al.* (Particle Data Group), *Prog. Theor. Exp. Phys.* **2022**, 083C01 (2022).
- [31] G. Duplančić and B. Melic, *JHEP* **11**, 138 (2015).
- [32] G. S. Bali, S. Collins, S. Dürr and I. Kanamori, *Phys. Rev. D* **91**, 014503 (2015).
- [33] R. N. Faustov, V. O. Galkin and X. W. Kang, *Phys. Rev. D* **101**, 013004 (2020).
- [34] N. R. Soni, M. A. Ivanov, J. G. Körner, J. N. Pandya, P. Santorelli and C. T. Tran, *Phys. Rev. D* **98**, 114031 (2018).

- [35] N. Offen, F. A. Porkert and A. Schäfer, *Phys. Rev. D* **88**, 034023 (2013).
- [36] K. Azizi, R. Khosravi and F. Falahati, *J. Phys. G* **38**, 095001 (2011).
- [37] P. Colangelo and F. De Fazio, *Phys. Lett. B* **520**, 78 (2001).
- [38] R. C. Verma, *J. Phys. G* **39**, 025005 (2012).
- [39] D. Melikhov and B. Stech, *Phys. Rev. D* **62**, 014006 (2000).
- [40] M. Ablikim *et al.* (BESIII collaboration), *Phys. Rev. Lett.* **122**, 121801 (2019).
- [41] M. Ablikim *et al.* (BESIII Collaboration), *Phys. Rev. D* **108**, 092003 (2023).
- [42] A. Bazavov *et al.* (Fermilab Lattice and MILC Collaborations), *Phys. Rev. D* **107**, 094516 (2023).
- [43] C. Aubin *et al.* (Fermilab Lattice, MILC and HPQCD Collaboration), *Phys. Rev. Lett.* **94**, 011601 (2005).
- [44] B. Chakraborty *et al.* (HPQCD Collaboration), *Phys. Rev. D* **104**, 034505 (2021).
- [45] H. Na, C. T. H. Davies, E. Follana, J. Koponen, G. P. Lepage and J. Shigemitsu, *Phys. Rev. D* **84**, 114505 (2011).
- [46] W. G. Parrott *et al.* (HPQCD Collaboration), *Phys. Rev. D* **107**, 014510 (2023).
- [47] J. Koponen *et al.* (HPQCD Collaboration), [arXiv:1208.6242 \[hep-lat\]](https://arxiv.org/abs/1208.6242).
- [48] J. Koponen *et al.* (HPQCD Collaboration), [arXiv:1305.1462 \[hep-lat\]](https://arxiv.org/abs/1305.1462).
- [49] N. Brambilla *et al.* *Eur. Phys. J. C* **74**, 2981 (2014).
- [50] J. A. Bailey *et al.* *Phys. Rev. D* **85**, 114502 (2012).
- [51] M. Ablikim *et al.* (BESIII Collaboration), *Phys. Rev. D* **97**, 012006 (2018).
- [52] M. Ablikim *et al.* (BESIII Collaboration), *Nucl. Instrum. Methods A* **614**, 345 (2010).
- [53] X. Li *et al.*, *Radiat. Detect. Technol. Methods* **1**, 13 (2017).
- [54] Y. X. Guo *et al.*, *Radiat. Detect. Technol. Methods* **1**, 15 (2017).
- [55] S. Agostinelli *et al.* (GEANT4 Collaboration), *Nucl. Instrum. Meth. A* **506**, 250 (2003).
- [56] K. X. Huang, Z. J. Li, Z. Qian, J. Zhu, H. Y. Li, Y. M. Zhang, S. S. Sun and Z. Y. You, *Nucl. Sci. Tech.* **33**, 142 (2022).
- [57] R. G. Ping, *Chin. Phys. C* **38**, 083001 (2014).
- [58] O. G. Tchikilev, *Phys. Lett. B* **471**, 400 (2000), Erratum: [*Phys. Lett. B* **478**, 459 (2000)].
- [59] M. Ablikim *et al.* (BESIII collaboration), “Measurement of the cross section for $e^+e^- \rightarrow D_s^\pm D_s^{*\mp}$ up to 4.7 GeV”, publication in preparation.
- [60] D. J. Lange, *Nucl. Instrum. Meth. A* **462**, 152 (2001); R. G. Ping, *Chin. Phys. C* **32**, 599 (2008).
- [61] J. C. Chen, G. S. Huang, X. R. Qi, D. H. Zhang and Y. S. Zhu, *Phys. Rev. D* **62**, 034003 (2000); R. L. Yang, R. G. Ping and H. Chen, *Chin. Phys. Lett.* **31**, 061301 (2014).
- [62] D. Cronin-Hennessy *et al.* (CLEO Collaboration), *Phys. Rev. D* **80**, 072001 (2009).
- [63] See Supplement Material at [URL will be inserted by publisher] for the systematic uncertainties in the BF measurements, the measured partial widths in different reconstructed q^2 intervals of the signal side, the statistical and systematic covariance matrices for different signal decays.
- [64] M. Ablikim *et al.* (BESIII Collaboration), *Phys. Rev. D* **83**, 112005 (2011).
- [65] M. Ablikim *et al.* (BESIII Collaboration), *Phys. Rev. Lett.* **122**, 071802 (2019).
- [66] M. Schmelling, *Phys. Scripta* **51**, 676 (1995).
- [67] T. Becher and R. J. Hill, *Phys. Lett. B* **633**, 61 (2006).
- [68] R. Aaij *et al.* (LHCb Collaboration), *Phys. Rev. Lett.* **119**, 101801 (2017).
- [69] M. Ablikim *et al.* (BESIII Collaboration), *Phys. Rev. Lett.* **122**, 061801 (2019).
- [70] M. Ablikim *et al.* (BESIII Collaboration), *Phys. Rev. Lett.* **122**, 011804 (2019).
- [71] M. Y. Khlopov, *Sov. J. Nucl. Phys.* **28**, 583 (1978).

APPENDICES

Table 1 summarizes the sources of the systematic uncertainties in the measurements of the branching fractions of $D_s^+ \rightarrow \eta^{(\prime)}\mu^+\nu_\mu$. In this table, the contributions to the systematic uncertainties listed in the top part are treated as correlated, while those in the bottom part are treated as uncorrelated.

Tables 2 and 3 give the weighted efficiency matrices averaged over all fourteen ST modes for $D_s^+ \rightarrow \eta\mu^+\nu_\mu$ and $D_s^+ \rightarrow \eta'\mu^+\nu_\mu$, respectively.

Tables 4 and 5 present the numbers of the

reconstructed events N_{DT}^i in data obtained from the MM² fits, the numbers of the produced events N_{prd}^i , and the measured partial decay rate $\Delta\Gamma_{msr}^i$ in different q^2 intervals for $D_s^+ \rightarrow \eta\mu^+\nu_\mu$ and $D_s^+ \rightarrow \eta'\mu^+\nu_\mu$, respectively.

Table 6 summarizes the statistical correlation matrices and relative uncertainties for the measured partial decay rates in different q^2 intervals for $D_s^+ \rightarrow \eta\mu^+\nu_\mu$.

Table 7 summarizes the systematic correlation matrices and relative uncertainties for the measured partial decay rates in different q^2 intervals for $D_s^+ \rightarrow \eta'\mu^+\nu_\mu$.

Table 1. Relative systematic uncertainties (in %) on the measurements of the branching fractions of $D_s^+ \rightarrow \eta\mu^+\nu_\mu$ and $D_s^+ \rightarrow \eta'\mu^+\nu_\mu$. The top and the bottom sections are correlated and uncorrelated, respectively. The uncertainty in the uncorrelated π^\pm tracking is obtained as the square root of the quadratic difference of the total uncertainty in the π^\pm tracking and the correlated portion. The last row of combined uncertainties are total uncertainties of $D_s^+ \rightarrow \eta\mu^+\nu_\mu$ and $D_s^+ \rightarrow \eta'\mu^+\nu_\mu$ after taking into account correlated and uncorrelated systematic uncertainties.

Source	$\eta_{\gamma\gamma}\mu^+\nu_\mu$	$\eta_{\pi^0\pi^+\pi^-}\mu^+\nu_\mu$	$\eta'_{\eta\pi^+\pi^-}\mu^+\nu_\mu$	$\eta'_{\gamma\pi^+\pi^-}\mu^+\nu_\mu$
ST D_s^- yields	0.5	0.5	0.5	0.5
μ^+ tracking	0.3	0.3	0.3	0.3
μ^+ PID	0.3	0.3	0.3	0.3
π^\pm tracking	—	1.2	0.6	0.6
π^\pm PID	—	0.4	0.4	0.4
π^0 or η reconstruction	1.1	1.1	0.8	—
Transition $\gamma(\pi^0)$ reconstruction	1.0	1.0	1.0	1.0
Smallest $ \Delta E $	1.0	1.0	1.0	1.0
Signal model	0.3	0.3	0.6	0.6
$M_{\eta^{(\prime)}\mu^+}$ and $M_{\eta^{(\prime)}\nu_\mu}$ requirements	0.7	0.7	2.4	2.4
Peaking background	0.7	0.7	1.0	1.0
π^\pm tracking	—	—	1.7	—
$\eta^{(\prime)}$ reconstruction	—	0.1	0.1	1.4
MM ² fit	0.2	0.7	1.2	1.2
Tag bias	0.5	0.2	0.2	0.2
MC statistics	0.3	0.3	0.3	0.3
E_γ^{\max} , $N_{\text{extra}}^{\text{char}}$, and $N_{\text{extra}}^{\pi^0}$ requirements	0.4	0.8	0.8	1.2
χ^2 requirement	—	—	—	1.6
Quoted branching fractions	0.5	1.1	1.3	1.4
Total	2.3	3.0	4.2	4.4
Combined	2.3		3.5	

Table 2. The efficiency matrices for $D_s^+ \rightarrow \eta\mu^+\nu_\mu$ averaged over all fourteen ST modes, where ε_{ij} represents the efficiency of events produced in the j -th q^2 interval and reconstructed in the i -th q^2 interval.

ε_{ij} (%)	$D_s^+ \rightarrow \eta_{\gamma\gamma}\mu^+\nu_\mu$								$D_s^+ \rightarrow \eta_{\pi^0\pi^+\pi^-}\mu^+\nu_\mu$							
	1	2	3	4	5	6	7	8	1	2	3	4	5	6	7	8
1	13.18	0.80	0.02	0.00	0.00	0.00	0.00	0.00	2.99	0.14	0.00	0.00	0.00	0.00	0.00	0.00
2	1.05	12.10	1.01	0.03	0.00	0.00	0.00	0.00	0.21	2.70	0.17	0.01	0.00	0.00	0.00	0.00
3	0.04	1.16	11.87	1.12	0.04	0.00	0.00	0.00	0.01	0.23	2.60	0.17	0.01	0.00	0.00	0.00
4	0.01	0.05	1.27	11.84	1.13	0.04	0.00	0.00	0.00	0.01	0.27	2.53	0.17	0.01	0.00	0.00
5	0.00	0.01	0.05	1.32	11.64	1.11	0.02	0.00	0.00	0.00	0.02	0.27	2.38	0.15	0.01	0.00
6	0.00	0.00	0.01	0.06	1.22	11.45	1.09	0.01	0.00	0.00	0.00	0.02	0.26	2.20	0.17	0.00
7	0.00	0.00	0.00	0.01	0.05	1.15	11.35	0.59	0.00	0.00	0.00	0.01	0.02	0.23	2.08	0.09
8	0.00	0.00	0.01	0.01	0.02	0.05	1.00	12.83	0.00	0.00	0.00	0.00	0.02	0.22	2.14	

Table 3. The efficiency matrices for $D_s^+ \rightarrow \eta' \mu^+ \nu_\mu$ averaged over all fourteen ST modes, where ε_{ij} represents the efficiency of events produced in the j -th q^2 interval and reconstructed in the i -th q^2 interval.

ε_{ij} (%)	$D_s^+ \rightarrow \eta'_{\eta\pi^+\pi^-} \mu^+ \nu_\mu$			$D_s^+ \rightarrow \eta'_{\gamma\pi^+\pi^-} \mu^+ \nu_\mu$		
	1	2	3	1	2	3
1	2.11	0.10	0.00	3.28	0.12	0.04
2	0.08	2.11	0.13	0.11	3.49	0.17
3	0.00	0.07	2.35	0.04	0.11	3.91

Table 4. The partial decay rates of $D_s^+ \rightarrow \eta \mu^+ \nu_\mu$ in different q^2 intervals of data, where the uncertainties of partial decay rates are statistical only.

i	1	2	3	4	5	6	7	8	
q^2 (GeV^2/c^4)	$(m_\mu^2, 0.2)$	$(0.2, 0.4)$	$(0.4, 0.6)$	$(0.6, 0.8)$	$(0.8, 1.0)$	$(1.0, 1.2)$	$(1.2, 1.4)$	$(1.4, q_{\max}^2)$	
$D_s^+ \rightarrow \eta \gamma \gamma \mu^+ \nu_\mu$	N_{DT}^i	403(26)	459(28)	397(27)	352(24)	303(21)	239(19)	188(19)	235(20)
	N_{prd}^i	2850(203)	3309(235)	2768(233)	2454(206)	2142(184)	1712(173)	1377(170)	1713(160)
	$\Delta \Gamma_{\text{msr}}^i$ (ns^{-1})	6.92(49)	8.04(57)	6.72(57)	5.96(50)	5.20(45)	4.16(42)	3.34(41)	4.16(39)
$D_s^+ \rightarrow \eta \pi^0 \pi^+ \pi^- \mu^+ \nu_\mu$	N_{DT}^i	97(13)	91(12)	83(12)	58(11)	70(10)	52(9)	35(8)	43(9)
	N_{prd}^i	3108(428)	2966(449)	2790(465)	1818(442)	2565(441)	1921(422)	1370(376)	1843(414)
	$\Delta \Gamma_{\text{msr}}^i$ (ns^{-1})	7.55(104)	7.20(109)	6.78(113)	4.41(107)	6.23(107)	4.67(103)	3.33(091)	4.48(100)

Table 5. The partial decay rates of $D_s^+ \rightarrow \eta' \mu^+ \nu_\mu$ in different q^2 intervals. Numbers in the parentheses are the statistical uncertainties.

i	1	2	3	
q^2 (GeV^2/c^4)	$(m_\mu^2, 0.3)$	$(0.3, 0.6)$	$(0.6, q_{\max}^2)$	
$D_s^+ \rightarrow \eta'_{\eta\pi^+\pi^-} \mu^+ \nu_\mu$	N_{DT}^i	64(11)	53(09)	28(07)
	N_{prd}^i	2944(503)	2300(425)	1138(317)
	$\Delta \Gamma_{\text{msr}}^i$ (ns^{-1})	7.15(122)	5.58(103)	2.76(077)
$D_s^+ \rightarrow \eta'_{\gamma\pi^+\pi^-} \mu^+ \nu_\mu$	N_{DT}^i	98(13)	106(13)	40(10)
	N_{prd}^i	2866(402)	2906(365)	912(265)
	$\Delta \Gamma_{\text{msr}}^i$ (ns^{-1})	6.96(98)	7.06(89)	2.22(64)

Table 6. Statistical and systematic correlation matrices and relative uncertainties for the measured partial decay rates of $D_s^+ \rightarrow \eta\mu^+\nu_\mu$ in different q^2 intervals.

Statistical correlation matrix																			
ρ_{ij}^{stat}	$D_s^+ \rightarrow \eta\gamma\gamma\mu^+\nu_\mu$								$D_s^+ \rightarrow \eta\pi^0\pi^+\pi^-\mu^+\nu_\mu$										
	1	2	3	4	5	6	7	8	1	2	3	4	5	6	7	8			
1	1.000	-0.144	0.015	-0.002	0.000	0.000	0.000	0.000	0.000	0.000	0.000	0.000	0.000	0.000	0.000	0.000	0.000	0.000	
2		1.000	-0.180	0.022	-0.003	0.000	0.000	0.000	0.000	0.000	0.000	0.000	0.000	0.000	0.000	0.000	0.000	0.000	
3			1.000	-0.203	0.025	-0.003	0.000	0.000	0.000	0.000	0.000	0.000	0.000	0.000	0.000	0.000	0.000	0.000	
4				1.000	-0.209	0.023	-0.003	0.000	0.000	0.000	0.000	0.000	0.000	0.000	0.000	0.000	0.000	0.000	
5					1.000	-0.200	0.023	-0.003	0.000	0.000	0.000	0.000	0.000	0.000	0.000	0.000	0.000	0.000	
6						1.000	-0.194	0.016	0.000	0.000	0.000	0.000	0.000	0.000	0.000	0.000	0.000	0.000	
7							1.000	-0.130	0.000	0.000	0.000	0.000	0.000	0.000	0.000	0.000	0.000	0.000	
8								1.000	0.000	0.000	0.000	0.000	0.000	0.000	0.000	0.000	0.000	0.000	
1									1.000	-0.120	0.010	-0.001	0.000	0.000	0.000	0.000	0.000	0.000	0.000
2										1.000	-0.150	0.015	-0.002	0.000	0.000	-0.001			
3											1.000	-0.173	0.013	-0.003	0.000	-0.002			
4												1.000	-0.179	0.015	-0.005	0.000			
5													1.000	-0.182	0.014	-0.002			
6														1.000	-0.188	0.010			
7															1.000	-0.135			
8																1.000			
Stat (%)	7.11	7.09	8.41	8.38	8.60	10.11	12.34	9.37	13.78	15.13	16.65	24.32	17.20	21.98	27.48	22.43			
Systematic correlation matrix																			
ρ_{ij}^{syst}	$D_s^+ \rightarrow \eta\gamma\gamma\mu^+\nu_\mu$								$D_s^+ \rightarrow \eta\pi^0\pi^+\pi^-e^+\nu_e$										
	1	2	3	4	5	6	7	8	1	2	3	4	5	6	7	8			
1	1.000	0.725	0.748	0.698	0.528	0.596	0.664	0.609	0.499	0.501	0.442	0.460	0.543	0.550	0.479	0.511			
2		1.000	0.748	0.409	0.748	0.251	0.660	0.416	0.654	0.273	0.692	0.217	0.300	0.528	0.550	0.535			
3			1.000	0.588	0.646	0.428	0.635	0.491	0.554	0.474	0.671	0.552	0.430	0.541	0.441	0.438			
4				1.000	0.223	0.778	0.521	0.595	0.227	0.643	0.190	0.701	0.624	0.430	0.245	0.296			
5					1.000	0.056	0.576	0.131	0.605	0.195	0.687	0.167	0.200	0.444	0.460	0.436			
6						1.000	0.373	0.563	0.103	0.580	-0.011	0.587	0.586	0.335	0.166	0.220			
7							1.000	0.392	0.476	0.368	0.448	0.316	0.393	0.454	0.416	0.419			
8								1.000	0.267	0.409	0.192	0.382	0.429	0.344	0.261	0.283			
1									1.000	0.481	0.799	0.253	0.421	0.654	0.630	0.729			
2										1.000	0.373	0.714	0.698	0.584	0.349	0.557			
3											1.000	0.311	0.311	0.598	0.570	0.596			
4												1.000	0.657	0.504	0.266	0.284			
5													1.000	0.572	0.487	0.519			
6														1.000	0.540	0.649			
7															1.000	0.568			
8																1.000			
Syst (%)	3.07	3.35	3.55	3.35	3.71	3.50	2.98	3.56	3.70	4.20	5.13	6.06	3.87	3.96	4.36	4.42			

Table 7. Statistical and systematic correlation matrices and relative uncertainties for the measured partial decay rates of $D_s^+ \rightarrow \eta' \mu^+ \nu_\mu$ in different q^2 intervals.

		Statistical correlation matrix					
ρ_{ij}^{stat}	$D_s^+ \rightarrow \eta'_{\eta\pi^+\pi^-} \mu^+ \nu_\mu$	$D_s^+ \rightarrow \eta'_{\gamma\pi^+\pi^-} \mu^+ \nu_\mu$					
		1	2	3	1	2	3
1	1.000	-0.086	0.004	0.000	0.000	0.000	
2		1.000	-0.088	0.000	0.000	0.000	
3			1.000	0.000	0.000	0.000	
1				1.000	-0.065	-0.018	
2					1.000	-0.073	
3						1.000	
Stat (%)	17.08	18.50	27.84	14.04	12.58	29.05	
Systematic correlation matrix							
ρ_{ij}^{syst}	$D_s^+ \rightarrow \eta'_{\eta\pi^+\pi^-} \mu^+ \nu_\mu$	$D_s^+ \rightarrow \eta'_{\gamma\pi^+\pi^-} \mu^+ \nu_\mu$					
		1	2	3	1	2	3
1	1.000	0.730	0.615	0.592	0.519	0.274	
2		1.000	0.960	0.500	0.488	0.502	
3			1.000	0.423	0.464	0.533	
1				1.000	0.631	0.460	
2					1.000	0.168	
3						1.000	
Syst (%)	4.22	4.74	5.98	4.43	6.46	8.19	